

COLLISIONS BETWEEN DARK MATTER CONFINED HIGH VELOCITY CLOUDS AND MAGNETIZED GALACTIC DISKS: THE SMITH CLOUD

JASON GALYARDT

Department of Physics and Astronomy, University of Georgia, Athens, GA 30602, USA

ROBIN L. SHELTON

Department of Physics and Astronomy, University of Georgia, Athens, GA 30602, USA

(Dated: November 19, 2015)
Draft version November 19, 2015

ABSTRACT

The Galaxy’s population of High Velocity Clouds (HVCs) may include a subpopulation that is confined by dark matter minihalos and falling toward the Galactic disk. We present the first magnetohydrodynamic simulational study of dark matter–dominated HVCs colliding with a weakly magnetized galactic disk. Our HVCs have baryonic masses of $5 \times 10^6 M_\odot$ and dark matter minihalo masses of $0, 3 \times 10^8$, or $1 \times 10^9 M_\odot$. They are modeled on the Smith Cloud, which is said to have collided with the disk 70 Myr ago. We find that, in all cases, the cloud’s collision with the galactic disk creates a hole in the disk, completely disperses the cloud, and forms a bubble-shaped structure on the far side of the disk. In contrast, when present, the dark matter minihalo continues unimpeded along its trajectory. Later, as the minihalo passes through the bubble structure and galactic halo, it accretes up to $6.0 \times 10^5 M_\odot$ in baryonic material, depending on the strengths of the magnetic field and minihalo gravity. These simulations suggest that if the Smith Cloud is associated with a dark matter minihalo and collided with the Galactic disk, the minihalo has accreted the observed gas. However, if the Smith Cloud is dark matter–free, it is on its first approach toward the disk. These simulations also suggest that the dark matter is most concentrated either at the head of the cloud or near the cloud, depending upon the strength of the magnetic field, a point that could inform indirect dark matter searches.

Keywords: dark matter — ISM: clouds — ISM: individual objects (Smith Cloud) — ISM: kinematics and dynamics — ISM: magnetic fields — methods: numerical

1. INTRODUCTION

The Milky Way has a population of gas clouds moving at high velocities relative to the Local Standard of Rest, the so-called High Velocity Clouds (HVCs). Such clouds have also been observed in or near to other large spiral galaxies (Westmeier et al. 2008, Miller et al. 2009) and the Local Group (Adams et al. 2013). They affect galaxy evolution by delivering material that can be used for making stars (Putman 2006, Lehner & Howk 2011, Putman et al. 2012, Fox et al. 2014) and, upon impact with the disk, by instigating star formation (Tenorio-Tagle 1981, Lepine & Duvert 1994, Izumi et al. 2014).

While the origins of HVCs are multiple and long debated (see, for example, Shapiro & Field 1976, Gardiner & Noguchi 1996, Wakker & van Woerden 1996), it is likely that some HVCs are dark matter–confined and represent a portion of the missing dark matter minihalo population (Blitz et al. 1999, Braun & Burton 2000). The extragalactic ultracompact HVCs in the ALFALFA survey, with dynamical masses far exceeding their HI masses, are excellent examples (Adams et al. 2013). These clouds have 10^5 to $10^6 M_\odot$ of HI mass and 10^7 to $10^8 M_\odot$ of total mass, making them as massive as dwarf galaxies. Even more massive (in HI) is the Smith Cloud (Smith 1963), an HVC that is claimed to have passed through the Milky Way’s outer disk (Lockman et al. 2008), and, owing to its having survived that passage, is suggested

to be gravitationally confined by dark matter (Nichols & Bland-Hawthorn 2009). Complex H, an even more massive HVC presently colliding with the outer disk of the Milky Way (Morras, Bajaja & Arnal 1998, Izumi et al. 2014), has also been suspected of harboring dark matter (Simon et al. 2006). Many dark matter–confined gaseous clouds must have collided with a galaxy the size of the Milky Way during its lifetime, calling attention to the question of how these collisions affect both the clouds and the galaxy.

The dynamical evolution of the cloud–galaxy collision depends on gravitational, magnetic, and hydrodynamic processes, often working against each other. The collision of a pure baryonic cloud with a non-magnetic galactic disk shocks and disrupts the cloud while punching a hole in the disk (Tenorio-Tagle 1981, Tenorio-Tagle et al. 1986). However, a magnetized disk can act as a barrier to penetration of the disk by a dark matter–free cloud (Santillán et al. 1999). Conversely, simulations in which the cloud has a dark matter cloud component and the disk has no magnetic field result in a coherent gas cloud appearing on the far side of the disk long after the collision (Nichols et al. 2014). The behavior of a dark matter–confined cloud when impacting a magnetized galactic disk has not been reported previously but is the topic of this work.

Using the three dimensional FLASH Eulerian multi-physics simulation package (Fryxell et al. 2000), we investigate the behavior of a dark matter–confined HVC as it collides with a weakly magnetized galactic disk similar

in field geometry and gas density to that of the Milky Way and compare with simulations that exclude one or both the minihalo and the magnetic field. We describe our simulation techniques and initial parameters in Section 2, discuss the results of individual simulations in Section 3, and summarize and discuss the ramifications for the Smith Cloud, infalling dark matter-dominated clouds, and dark matter searches in Section 4.

2. METHODOLOGY AND SIMULATIONS

Our cloud is patterned after the Smith Cloud, whose tip is currently located at $(l, b) \approx (38^\circ.67, -13^\circ.41)$ and whose heliocentric distance is 12.3 ± 1.4 kpc (Lockman et al. 2008). Its hydrogen mass exceeds $2 \times 10^6 M_\odot$, evenly split between atomic (Lockman et al. 2008) and ionized (Hill et al. 2009) hydrogen. The observations by Hill et al. (2013) of a significant line of sight enhancement to the magnetic field around the Cloud indicate that it is interacting with the local Galactic magnetic field. Following Nichols et al. (2014), we model the progenitor cloud as a sphere of 0.5 kpc radius with an initial hydrogen number density of 0.4 cm^{-3} , which results in a total baryonic mass of $5.0 \times 10^6 M_\odot$. In our model, the cloud is initially in pressure equilibrium with the ambient medium, resulting in an average interior cloud temperature of 880 K. The density and temperature transition smoothly from those at the cloud center to those of the ambient material at the cloud’s periphery. In order to give the cloud time to evolve dynamically in the gaseous halo environment prior to the collision, we start the cloud 10 kpc above the midplane of the Galactic disk, at a galactocentric radius of 13 kpc (the galactocentric radius of its prior impact with the disk, as estimated by Lockman et al. (2008)), with a downward velocity of 200 km s^{-1} .

For numerical tractability, we model the dark matter minihalo using the Einasto density profile (Einasto 1965, Merritt et al. 2006): $\rho(r) = \rho_e \exp\{-d_n[(r/r_e)^{1/n} - 1]\}$, where ρ_e defines the nominal density, r_e defines the half-mass radius for an infinite dark matter distribution, n defines the ‘shape’ of the distribution, and $d_n \approx 3n - 1/3 + 0.0079/n$, for $n \gtrsim 0.5$ (Merritt et al. 2006). The models of Nichols & Bland-Hawthorn (2009) suggest that, in order for the Smith Cloud to survive its passage through the Galactic disk, it must have a dark matter mass of 2×10^8 to $1 \times 10^9 M_\odot$. In the interest of exploring the sensitivity to the minihalo mass, we sample three minihalo masses: 0, 3×10^8 , and $1 \times 10^9 M_\odot$. For consistency with the shape parameters used in Nichols & Bland-Hawthorn (2009), we use common values of $r_e = 1.0$ kpc, and $n = 1/0.17$ in all simulations that include a dark matter minihalo. For the smaller mass minihalos, we use $\rho_e = 9.79 \times 10^{-3} M_\odot \text{ pc}^{-3}$; for the more massive minihalos, we use $\rho_e = 3.27 \times 10^{-2} M_\odot \text{ pc}^{-3}$. We model the dark matter in FLASH by approximately ten thousand massive, collisionless particles. The particles’ initial positions are generated randomly from the appropriate Einasto density profile, centered upon the baryonic cloud. In order to promote minihalo shape stability, we generate a peculiar velocity for each particle according to a Maxwell-Boltzmann distribution. The total velocity of each particle is set as the sum of the random peculiar velocity and the minihalo group velocity of 200 km s^{-1} toward the disk.

We model the Galaxy’s ISM as a cool disk (Dehnen

& Binney 1998) and hot halo (Miller & Bregman 2013), composed entirely of atomic hydrogen. We set the gas density distribution, common to all our simulations, as the sum of the disk and halo gas densities. The density at the midplane within our simulation domain varies smoothly between 9.8 and 6.2 cm^{-3} with increasing galactocentric radius. The density falls smoothly with height, as set by the component models of Dehnen & Binney (1998) and Miller & Bregman (2013). The temperature is 1100 K at the Galactic midplane and it smoothly rises with height above the plane until it reaches 1×10^6 K at about 1.5 kpc above the midplane.

We model the distribution of mass within the Galaxy as the superposition of the above-described gaseous components, a stellar component that includes contributions from the bulge, thin and thick disks (McMillan 2011), and halo (Jurić et al. 2008), and a dark matter component whose distribution was adopted from Navarro, Frenk, & White (1996) with parameters from McMillan (2011). The masses of these components sum to $1.6 \times 10^{12} M_\odot$.

We used this distribution of mass to calculate the Galaxy’s gravitational acceleration, $\mathbf{g}(R, z)$, as a function of position in cylindrical polar coordinates. The galactic gravitational acceleration in our simulations is thus self-consistent with the observation-based mass distribution in our model. In order to obtain the gravitational acceleration at any spatial point, we first calculate the 3D gravitational acceleration due to our mass model on an R - z grid with azimuthal symmetry and dimensions of $N \times M$, resulting in $\mathbf{g}_{nm}(R_n, z_m) = \sum_i \mathbf{g}_{nm}^{(i)} \hat{\mathbf{e}}_i$, with the $\hat{\mathbf{e}}_i$ representing the Cartesian unit vectors. We then fit the grid of $\mathbf{g}_{nm}^{(i)}$ with a separate bivariate B-spline for each vector component, i . Our model’s mass distribution extends out to a galactocentric radius of 30 kpc and height of ± 200 kpc.

For the runs that include a Galactic magnetic field, we implement the coherent magnetic field component of Jansson & Farrar (2012a) within the simulation domain. This model includes spiral geometry in the disk, transitioning to a toroidal geometry for the halo; it also includes an ‘X’-shaped poloidal component. It is important to note that the coherent field is roughly 15 to 20% of the total field; the remaining components of the Jansson & Farrar (2012b) model are the isotropic random and striated random fields. The latter two components of the magnetic field are not included in the simulations presented here due to numerical instabilities associated with turbulent flow of the random field components under an ideal MHD evolution framework. Thus, we characterize the magnetic field used in our simulations as weak.

We use FLASH version 4.2 in three dimensions with a Cartesian coordinate system. The procedural evolution of the runs within FLASH varied slightly, employing either the unsplit hydrodynamic or the unsplit staggered mesh ideal MHD solver, as appropriate. We use the adiabatic ideal gas equation of state (EOS) with an adiabatic index γ of 5/3. We neglect cooling. In order to account for both the dynamic internal mass and the static external Galactic mass, we implemented a new gravity solver in FLASH that combines the built-in Barnes-Hut Tree Poisson solver for self-gravity with the interpolated gravitational acceleration due to our Galactic mass model,

Table 1

Simulation Runs: Physical Effects and Baryonic Cloud Masses

Run	$m_{DM} [M_\odot]$	B -field	$m_{cloud}(t) [M_\odot]$		
			t_1	t_2	t_3
1	0.0	No	3.2×10^6	3.9×10^5	2.1×10^5
2	0.0	Yes	3.2×10^6	5.2×10^5	3.7×10^5
3	3.0×10^8	No	4.1×10^6	2.2×10^5	9.4×10^4
4	3.0×10^8	Yes	4.2×10^6	1.4×10^5	2.5×10^4
5	1.0×10^9	No	4.1×10^6	6.2×10^5	7.9×10^5
6	1.0×10^9	Yes	4.1×10^6	4.6×10^5	6.0×10^5

Note. — For all runs, the initial baryonic cloud mass, $m_{cloud}(t_0)$, was $5.0 \times 10^6 M_\odot$. See the text for the method used to calculate $m_{cloud}(t)$ for later times. The sampling times for baryonic mass were as follows: $t_1 = 35$ Myr for all runs; $t_2 = 52$ Myr for Runs 1 & 2 and $t_2 = 45$ Myr for Runs 3–6; $t_3 = 75$ Myr for all runs. The second epoch, t_2 , differs in sampling time according to dark matter content: after the collision, the dark matter-free runs require an additional 7 Myr to develop to the same level of maturity as those with minihalos.

yielding the total gravitational acceleration. In our simulations, we ignored the radial component of the Galaxy’s gravitational acceleration, setting $\mathbf{g}(R, z) = g_z(R, z)\hat{z}$, in order to minimize radial motion and thus keep the simulation domain smaller and the spatial resolution acceptable with the available computational resources. The self-gravity component of the acceleration vector is unrestricted in direction. While the baryonic mass in the simulation domain contributes to both the self-gravity and the external gravity source (via the Galactic mass model), the effect of this double counting on the simulation dynamics is expected to be small. The cloud’s dark matter minihalo and the Galactic dark matter halo are the dominant components of the self- and external gravity fields, respectively, and are not affected by this double counting.

We performed a suite of simulations whose identification numbers, dark matter mass, and presence of magnetic field are listed in Table 1. Table 1 also notes the baryonic mass of the cloud, $m_{cloud}(t)$, at various stages of evolution. Our method for calculating the baryonic cloud mass from the simulation data was to integrate the gas density in three dimensions over a sphere of 0.5 kpc radius. The sphere was centered on the dark matter minihalo barycenter for Runs 3–6. For completeness, we performed our cloud mass calculation upon the runs without minihalos and listed the results along with those of the other runs in Table 1. For these runs (Runs 1 & 2), the sphere was centered either on the baryonic cloud, or, if no cloud was obvious, on the lowest z point of the bubble’s shell (thus the point most similar to that in Runs 3–6) for pre-collision and post-collision epochs, respectively. We did not subtract any ambient baryonic mass that the sphere contained. The dark matter-free runs develop at a slower rate after the collision than do the runs with minihalos, requiring an additional 7 Myr to reach the same level of maturity. Therefore, the epoch labeled t_2 in Table 1 corresponds to a simulation time of 52 Myr for Runs 1 & 2 and 45 Myr for Runs 3–6. Epochs labeled t_1 and t_3 correspond to 35 and 75 Myr, respectively, for all runs.

Figure 1 shows the initial conditions for all six runs in slices through the $y = 0$ plane. For computational efficiency, we restrict the simulation domain to a

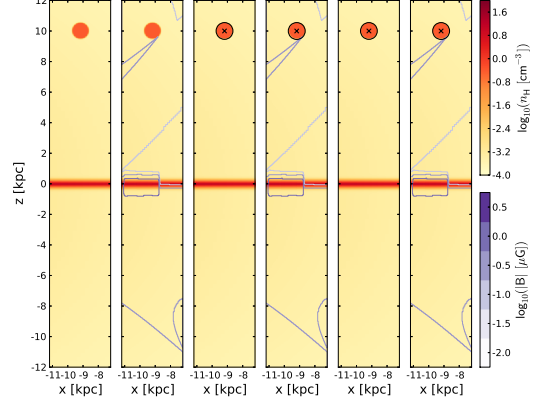


Figure 1. Initial conditions for each simulation along slices through the $y = 0$ plane. \log_{10} of hydrogen number density is represented by the continuous color scale. \log_{10} of magnetic field strength is represented by contours. The dark matter barycenter is marked with an ‘X’ and a circle at the half-mass radius. From left to right, the panels show Runs 1–6, as in Table 1.

4 kpc \times 4 kpc \times 24 kpc region of the Galaxy. The Galactic magnetic field model of Jansson & Farrar (2012a) has azimuthal variations in strength and direction of the field. We chose the galactocentric azimuthal angle to roughly agree with that of the point of impact 70 Myr ago shown in Nichols & Bland-Hawthorn (2009), Figure 3. The minihalos are necessarily constrained by the size of the domain and fill spheres of 2 kpc radius (the domain half-width). In Figure 1, the minihalo barycenters are indicated by the ‘X’ markers, and their simulation domain half-mass radii (distinct from r_e) are shown as black circles.

3. RESULTS

All six clouds behave similarly as they fall through the halo. This can be seen in Figure 2 which shows the clouds at epoch t_1 (35 Myr), just before impact. As they pass through the halo, the clouds lose material due to ram pressure stripping. By epoch t_1 the clouds with minihalos have lost 16–18% of their original baryonic mass, while those without have lost $\sim 36\%$ (see Table 1). During this stage, the effect of the weak magnetic field is merely to become swept up and wrapped around the cloud. This is similar to the behavior in the 2D MHD simulations of Konz et al. (2002).

Each of the clouds approaches the disk with a similar velocity ($\sim 300 \text{ km s}^{-1}$). However, the dark matter confined clouds are more compact and contain more baryonic mass and so carry larger kinetic energy densities than the dark matter-free clouds. The collision of the cloud with the Galactic disk occurs at 36 Myr for those runs with a minihalo, and 37 Myr for the dark matter-free runs. At the moment of collision, the minihalo separates from the cloud gas and continues, unhindered, through the Galactic disk. During the collision, the gas cloud ceases to exist as it mixes with and transfers momentum to the disk gas. This results in a hole in the disk and a long-lived, bubble-shaped structure filled with moderately dense (~ 0.1 to $\sim 3 \text{ H cm}^{-3}$), cool gas ($\sim 1000 \text{ K}$) below the disk, as shown in Figure 3 at 52 Myr for Runs 1 & 2 and 45 Myr for Runs 3–6 (epoch t_2). These structures are composed of a mixture of gas from both the cloud

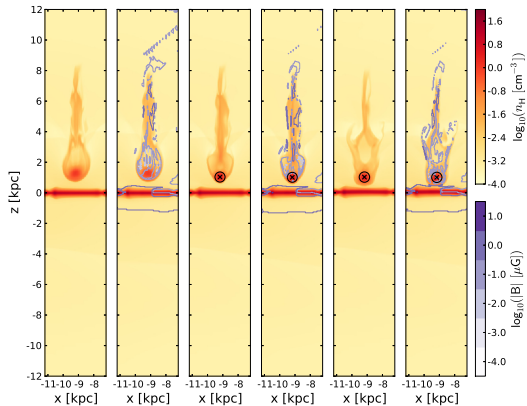


Figure 2. Same as Figure 1, but for epoch t_1 , equivalent to $t = 35\text{Myr}$ for all runs.

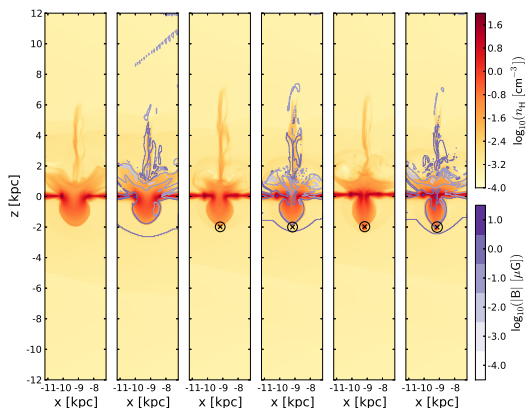


Figure 3. Same as Figure 1, but for epoch t_2 , equivalent to $t = 52\text{Myr}$ for Runs 1 & 2 and $t = 45\text{Myr}$ for Runs 3–6.

and the disk, with the majority of their mass originating from the disk. Tenorio-Tagle et al. (1986) found similar structures in 2D hydrodynamic simulations of dark matter-free clouds colliding with the Galactic thin disk.

Over time, each minihalo gravitationally accretes gas from its surroundings. By epoch t_2 , the minihalos have trapped an amount of baryonic mass equivalent to 2.8 to 12% of the original baryonic cloud mass. See Table 1.

For runs 3–6, the magnetohydrodynamic and dark matter gravitational forces continue to influence the evolution of the gas density distribution long after the collision (Figure 3 to Figure 4). The minihalo’s gravity continues to tug on the gas at the bottom of this bubble-shaped structure while magnetohydrodynamic forces slow its horizontal expansion. Although the gravitational tug elongates this structure in simulations 3–6 relative to those in Runs 1 & 2, it cannot do so indefinitely. Eventually it pulls off a small, comet-shaped fragment. In Run 4, the fragment completely separates from the bubble-shaped structure, but in Runs 3, 5, and 6, a drip-line of gas connects the fragment to the bubble-shaped structure. In Runs 3 & 4, where the minihalo mass is $3 \times 10^8 M_\odot$, the newly accreted baryonic mass is very small, only 1.9 and 0.50% of the original baryonic mass, respectively. In contrast, the $3\times$ more massive

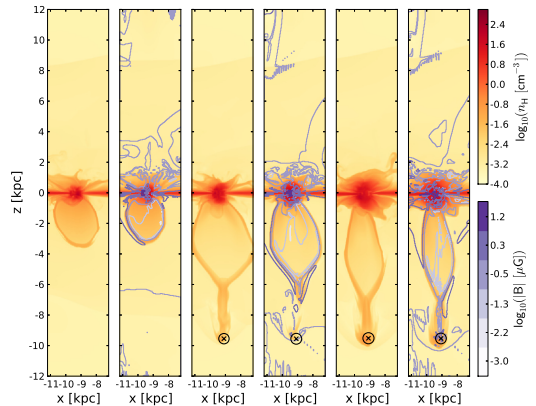


Figure 4. Same as Figure 1, but for epoch t_3 , equivalent to $t = 75\text{Myr}$ for all runs.

dark matter minihalos in Runs 5 and 6 allow them to accrete gas from the surrounding Galactic halo, bringing the mass of their freshly formed clouds to 16 and 12%, respectively, of their original baryonic masses by epoch t_3 (75 Myr).

4. SUMMARY AND DISCUSSION

It has been suggested that a dark matter minihalo “shepherded” the Smith Cloud through the outer disk, that the minihalo then ballistically traveled through the halo, dragging the gas cloud along with it, and that they are now poised to fall into the disk again. In order to examine the passage of a dark matter enshrouded Smith Cloud-sized gas cloud through the outer portion of a magnetized galactic disk, we performed a series of simulations, some with a weak galactic magnetic field and some with a dark matter minihalo. In all cases, the cloud’s collision with the disk punches a hole in the disk, obliterates the cloud, and produces a large bubble-shaped distribution of cool gas below the disk. When a dark matter minihalo is present, it gathers material from the bubble into a comet-shaped density enhancement that travels with the minihalo. In addition, if the minihalo is extremely massive, it later accretes some gas from the Galactic halo, and the head of the cloud likely remains co-located with the minihalo. It is thus a prime target for dark matter signal searches. It should be noted that the simulation with a low mass minihalo and a galactic magnetic field (Run 4) shows indications that the gas currently confined by the minihalo may be stripped out by the galactic magnetic field on time scales longer than we simulated, resulting in the minihalo leading the cloud. However, in none of our cases is the final mass of baryonic material accompanying the minihalo more than 16% of the primordial cloud mass or 40% of the observed Smith Cloud mass.

The presence of even a weak Galactic magnetic field reduces the amount of gas that accompanies the minihalo, irrespective of minihalo mass. It should be noted, however, that only the coherent component of the Galactic magnetic field is modeled in this work. If the random components of the Jansson & Farrar (2012b) model were to be included as well (for fixed minihalo mass), then the net strength of the magnetic field in the disk and halo would have been ~ 6 times greater and would have

resulted in a smaller final cloud mass.

Under the premise that the Smith Cloud previously passed through the Galactic disk accompanied by a dark matter minihalo, our simulations indicate that the observed gas comprising the Smith Cloud must have been accreted onto the minihalo since its disk passage. This implies that the metallicity of the Smith Cloud should be similar to that of the Galactic ISM along its trajectory, rather than primordial in nature. Our simulations favor the larger mass minihalo under this premise, as it is likely that the Galactic magnetic field would prevent the lower mass minihalo from accumulating the amount of gas observed.

On the other hand, if the premise is not correct and the Smith Cloud was not accompanied by a dark matter minihalo, then it would not have survived passage through the Galactic disk, irrespective of the presence of a magnetic field. In that case, the Smith Cloud must currently be on its first descent into the disk.

From the Galactic point of view, the remnant bubbles of HVC-disk collisions grow to heights of 3 to 7 kpc. Based in extended simulation times on Runs 1, 3, and 5, these structures should survive for ~ 50 Myr (for HVCs without dark matter) to ~ 60 Myr (for HVCs with dark matter). If HVC material were to collide with a weakly magnetized galactic disk at the rate of $1 M_{\odot} \text{ yr}^{-1}$ (Shull et al. 2009, Lehner & Howk 2011) in $5 \times 10^6 M_{\odot}$ clouds as in our simulations, we would expect ~ 10 to 12 extant bubbles at any given time, for purely dark matter-free and purely dark matter-rich HVC-disk collisions, respectively. The number of HVC collision-driven bubbles would be affected by the actual Galactic magnetic field strength (a stronger field would result in fewer bubbles at any given time), the number of HVCs reaching the disk, the baryonic mass and size of impacting HVCs, and the proportion of gas-bearing minihalos on collisional orbits.

Our simulated HVC collision-driven bubble structures are reminiscent of the supergiant shells (SGSs) observed in the Milky Way (Heiles 1984) and elsewhere (e.g., LMC: Book et al. 2008; M31: Brinks & Bajaja 1986; IC 2574: Walter & Brinks 1999). Young SGSs are likely to contain hot gas (McCray & Kafatos 1987) and have enhanced metallicities due to supernova activity. Evolved SGSs are likely to have cool interiors due to metal line emission (MacLow 2000) or blowouts (McCray & Kafatos 1987). In contrast, we predict that HVC collision-driven structures would have cool interiors and galactic or subgalactic metallicities. In principle, one could perform a search for HVC collision-driven shell structures within the population of Galactic or extragalactic SGSs. Using the discriminants outlined above, such a search may allow one to identify candidate structures and constrain the rate of infalling gas-bearing minihalos.

Our simulations show that the majority of the infalling HVC gas will merge into the Galactic disk. Although the collision blows an enormous bubble, most of the bubble material will eventually fall back into the disk. Only a small amount of HVC plus Galactic material will be carried away with the dark matter minihalo. HVC-disk collisions are thus efficient mechanisms for contributing gas to the Galactic disk, supporting future star formation.

We would like to acknowledge J. Bland-Hawthorn, G. Farrar, A. Hill, and F. J. Lockman for useful discussions and the anonymous referee for insightful comments. This study was supported in part by resources and technical expertise from the Georgia Advanced Computing Resource Center, a partnership between the University of Georgia's Office of the Vice President for Research and Office of the Vice President for Information Technology. This work was supported by NASA grant 10-21-RR185-451.

REFERENCES

- Adams, E. A. K., Giovanelli, R., & Haynes M. P. 2013, *ApJ*, 768, 77
- Blitz, L., Spergel, D. N., Teuben, P. J., Hartmann, D., & Burton, W. B. 1999, *ApJ*, 514, 818
- Book, L. G., Chu, Y. H., & Gruendl, R. A. 2008 *ApJS* 175 165
- Braun, R., & Burton, W. B. 2000, *A&A*, 354, 853
- Brinks, E., & Bajaja, E. 1986, *A&A*, 169, 14
- Dehnen, W. & Binney, J. 1998, *MNRAS*, 294, 429
- Drlica-Wagner, A., Gómez-Vargas, G. A., Hewitt, J. W., Linden, T., & Tibaldo, L. 2014, *ApJ*, 790, 24
- Einasto J. 1965, *Tr. Astrofiz. Inst. Alma-Ata*, 5, 87
- Fox, A., et al. 2014, *ApJ*, 787, 147
- Fryxell, B., Olson, K., Ricker, P., et al. 2000, *ApJS*, 131, 273
- Gardiner, L. T., & Noguchi, M. 1996, *MNRAS*, 278, 191
- Heiles, C. 1984, *ApJS* 55, 585
- Hill, A. S., Haffner, L. M., & Reynolds, R. J. 2009, *ApJ* 703, 1832
- Hill, A. S., Mao, S. A., Benjamin, R. A., Lockman, F. J., & McClure-Griffiths, N. M. 2013, *ApJ* 777, 55
- Izumi, N., Kobayashi, N., Yasui, C., Tokunaga, A. T., Saito, M., & Hamano, S. 2014, *ApJ*, 795, 66
- Jansson, R., & Farrar, G. R. 2012, *ApJ*, 757, 14
- Jansson, R., & Farrar, G. R. 2012, *ApJL*, 761, L11
- Jurić, M., Ivezić, Z., Brooks, A., et al. 2008, *ApJ*, 673, 864
- Konz, C., Brüns, C., & Birk, G. T. 2002, *A&A* 391, 713
- Lepine, J. R. D. & Duvert, G. 1994, *A&A* 286, 60
- Lehner, N. & Howk, C. 2011, *Science*, 334, 955
- Lockman, F. J., Benjamin, R. A., Heroux, A. J., & Langston, G. I. 2008, *ApJ*, 679, L21
- MacLow, M.-M. 2000, *RMxAC*, 9, 273
- McCray, R. & Kafatos, M. 1987, *ApJ*, 317, 190
- McMillan, P. J. 2011, *MNRAS*, 414, 2446
- Merritt, D., Graham, A.W., Moore, B., Diemand, J., & Terzić, B. 2006, *AJ*, 132, 2685
- Miller, E. D., Bregman, J. N., & Wakker, B. P. 2009, *ApJ*, 692, 470
- Miller, M. J. & Bregman, J. N. 2013, *ApJ*, 770, 118
- Morras, R., Bajaja, E., & Arnal, E. M. 1998, *A & A*, 334, 659
- Navarro, J. F., Frenk, C., & White, S. D. 1996, *ApJ*, 462, 563
- Nichols M. & Bland-Hawthorn, J. 2009, *ApJ*, 707, 1642
- Nichols, M., Mirabal, N., Agertz, O., Lockman, F. J., & Bland-Hawthorn, J. 2014, *MNRAS*, 442, 2883
- Putman, M. E. 2006, *ApJ*, 645, 1164
- Putman, M. E., Peek, J. E. G., & Jounge, M. R. 2012, *ARAA*, 50, 491
- Santillán, A., Franco, J., Martos, M., & Kim, J. 1999, *ApJ*, 515, 657
- Shapiro, P. R., & Field, G. B. 1976, *ApJ*, 205, 762
- Shull, J. M., Jones, J. R., Danforth, C. W., & Collins, J. A. 2009, *ApJ*, 699, 754
- Simon, J. D., Blitz, L., Cole, A. A., Weinberg, M. D., & Cohen, M. 2006, *ApJ*, 640, 270
- Smith G. P., 1963, *Bull. Astron. Inst. Neth.*, 17, 203
- Tenorio-Tagle, G. 1981, *A&A*, 94, 338
- Tenorio-Tagle, G., Bodenheimer, P., Rozyczka, M., Franco, J. 1986, *A&A*, 170, 107
- Wakker, B. P. & van Woerden, H. 1996, *ARA & A*, 35, 217
- Walter, F., & Brinks, E. 1999, *AJ*, 118, 273
- Westmeier, T., Brüns, C., & Kerp, J. 2008, *MNRAS*, 390, 1691